

1 Synergistic effects of previous winter NAO and ENSO 2 on the spring dust activities in North China

3 Falei Xu¹, Shuang Wang¹, Yan Li², and Juan Feng¹

4 ¹State Key Laboratory of Remote Sensing Science, Faculty of Geographical Science, Beijing
5 Normal University, Beijing, China

6 ²Key Laboratory for Semi-Arid Climate Change of the Ministry of Education, College of
7 Atmospheric Sciences, Lanzhou University, Lanzhou, China

8 **Correspondence:** Juan Feng (fengjuan@bnu.edu.cn)

9 Abstract

10 Dust plays an important role in influencing global weather and climate via impacting the Earth's
11 radiative balance. Based on the atmospheric and oceanic datasets during 1980-2022, the impacts of
12 preceding winter North Atlantic Oscillation (NAO) and El Niño-Southern Oscillation (ENSO) on
13 the following spring dust activities over North China are explored. It is found that both NAO and
14 ENSO exert significant effects in influencing the dust activities over North China, particularly
15 during their negative phases. A synergistic influence on the dust activities in North China is observed
16 when both NAO and ENSO are in negative phase, with their combined impacts exceeding that of
17 either factor alone. The previous winter NAO exhibits significant impacts on the sea surface
18 temperatures (SST) in the North Atlantic, associating with an anomalous SST tripole pattern. Owing
19 to the persistence of SST, these anomalies can extend into the following spring, when anomalous
20 atmospheric teleconnection wave trains would be induced, thereby influencing the dust activities in
21 North China. ENSO, on the one hand, directly impacts dust activities in North China by modulating
22 the circulation in the Western North Pacific (WNP). Moreover, ENSO enhances the NAO's effect
23 on the North Atlantic SST, explaining their synergistic effects on the dust activities over North China.
24 This study explains the combined role of NAO and ENSO on the dust weather over North China,
25 providing one season ahead signals for the forecast of spring dust activities in North China.

26

27 **1. Introduction**

28 Dust, as one of the most significant natural aerosols in the atmosphere, is of great importance
29 to the global radiative balance with its light-absorbing properties, exerting a crucial role in climate
30 change (e.g., Lou et al., 2017; Li et al., 2022; Kok et al., 2023). Moreover, dust not only influences
31 its source regions but also extends its impact across oceans via teleconnections driven by
32 atmospheric circulation. This transboundary transport affects ocean-atmosphere interactions and has
33 a profound impact on the Earth's climate system (Huang et al., 2015). Dust weather, resulting from
34 regional dust surges, poses a formidable threat to socio-economic development, natural ecological
35 environment, as well as human health and safety (Zhao et al., 2020; Li et al., 2023). The Gobi Desert
36 in East Asian, especially for the Mongolian Plateau and Northern China, is a major source of dust
37 (Chen et al., 2023; Hu et al., 2023), contributing approximately 70% of Asia's total dust emissions
38 (Zhang et al., 2003). Given that China is one of the countries profoundly impacted by dust disasters
39 (Fan et al., 2018), exploring the variations in dust disasters in China is of significant scientific and
40 practical importance.

41 Northern China, primarily affected by dust weather, experienced over 80% of its dust events
42 during boreal spring (March-May) (Shao et al., 2023). In spring, besides the dust source regions
43 over China (mainly Xinjiang and Inner Mongolia), North China also exhibited high dust
44 concentrations and significant dust interannual variability (Liu et al., 2004; Ji and Fan, 2019).
45 Additionally, as a crucial center for politics, economy, and population, it is meaningful to investigate
46 the variations of spring dust weather over North China and to explore the relevant physical
47 mechanisms. Previous studies have revealed that the frequency of dust events in China exhibits
48 strong interannual and interdecadal characteristics, with a high frequency from the 1950s to 1970s,
49 a low frequency from the 1980s to 1990s, and a remarkable increase after 2000 (Zhu et al., 2008; Ji
50 and Fan, 2019). On interdecadal time scales, climate oscillations such as the Atlantic Multidecadal
51 Oscillation (AMO), Pacific Decadal Oscillation (PDO), as well as Antarctic Oscillation (AAO) can
52 influence the dust activities by affecting the climate background. For instance, the positive phase of
53 PDO is favorable for less dust weather by influencing the westerly belt, leading to weaker dust
54 activities (uplift and deposition) in the Asian region (Gong et al., 2006). The AMO plays a role in
55 affecting the global aridification process by altering the thermal properties between land and sea
56 (Huang et al., 2017). Additionally, the AAO may substantially regulate dust weather in China by
57 affecting the frequency of dust in East Asia through the interaction of meridional circulations
58 between the Northern and Southern Hemispheres (Ji and Fan, 2019).

59 On the interannual scale, a weaker East Asian winter monsoon (EAWM) is associated with
60 anomalous circulation over the Gobi and Taklamakan deserts facilitate transport of dust,
61 consequently increasing dust concentrations in China (Lou et al., 2016). The variations of the sea
62 ice coverage in the Barents Sea can significantly influence the intensity and frequency of dust
63 weather in China by influencing cyclone generation and thermal instability in North China (Fan et
64 al., 2018). The North Atlantic Oscillation (NAO) can exert a substantial influence on the spring dust
65 weather in North China by modulating the zonal wave train from the Atlantic to the Pacific at mid-
66 latitudes in the Northern Hemisphere, as well as the sea level pressure (SLP) gradient in the Tarim
67 Basin in China (Zhao et al., 2013). On the synoptic scale, the NAO exerts a vital influence on the
68 emergence and evolution of dust weather in North China, via its impact on the transport of transient
69 wave flux and modifications in atmospheric circulation (Li et al., 2023). Beyond extratropical
70 signals, tropical variabilities, such as El Niño–Southern Oscillation (ENSO), also significantly
71 modulated dust activities in China by regulating variations in large-scale circulation, precipitation,
72 and temperature over East Asia (Yang et al., 2022a), as well as in Saudi Arabia (Yu et al., 2015),
73 Central Asia (Xi and Sokolik, 2015), and North America (Achakulwisut et al., 2017).

74 From the aforementioned studies on the dust activities in China, it is seen that the NAO and
75 ENSO are two important factors, with a focus on their individual effects on the dust weather in
76 China. However, as one of the most significant climate variabilities in the extratropical and tropical
77 regions, respectively, the NAO and ENSO often co-occur and have complex interactions (López-
78 Parages et al., 2015). It is found that ENSO can influence the climate near the North Atlantic through
79 atmospheric forcing of the Pacific North America teleconnection (Wallace and Gutzler, 1981).
80 During the early winter of El Niño events, strong convective anomalies in the tropical Indian Ocean-
81 Western Pacific (Abid et al., 2021) and the Gulf of Mexico-Caribbean Sea (Ayarzagüena et al., 2018)
82 can trigger Rossby wave trains reaching the North Atlantic, leading to positive NAO signals, and
83 vice versa. Furthermore, the stratosphere, serving as an energy transmission channel, may also be
84 an important pathway for ENSO to influence the NAO (Jiménez-Esteve and Domeisen, 2018).
85 Moreover, observations and numerical simulations have demonstrated that NAO signal can induce
86 a Gill-Matsuno pattern in the tropical region of southern Eurasia, inducing a decadal enhancement
87 in the linkage between the East Asian summer monsoon (EASM) and ENSO (Wu et al., 2012).
88 When the NAO is in its positive phase, intensified northeasterlies are observed over tropical North
89 Atlantic, resulting in increased low-level moisture content and precipitation in the tropical North
90 Atlantic, paralleling with stronger convection and enhanced ENSO impact (Ding et al., 2023). These
91 researches highlight the connections and interactions between NAO and ENSO, underscoring the

92 necessity of considering their synergistic effects on the dust activities in North China.

93 The synergistic effect refers to the phenomenon where the combined impacts of two or more
94 factors is significantly greater than their individual role (Li et al., 2019). It is found that there are
95 synergistic effects in the impact of NAO and ENSO on the weather and climate over China. The
96 NAO can facilitate the development of the subpolar teleconnection across northern Eurasia
97 downstream, leading to anomalies in the high-pressure systems over the Ural Mountains and the
98 Sea of Okhotsk, which in turn affect the EASM (Wang et al., 2000). Meanwhile, ENSO exerts
99 significant impact on the convective activities in the central Pacific and induces alterations in the
100 equatorial circulation via the Pacific-East Asia teleconnection, further affecting the atmospheric
101 circulation and sea surface temperature (SST) in the Western North Pacific (WNP), ultimately
102 influencing the intensity of EASM (Wang et al., 2000). Therefore, the synergistic effects of these
103 factors can result in pronounced impacts on the EASM (Wu et al., 2009). During El Niño events,
104 SST in the central and eastern equatorial Pacific rises, enhancing convective activity near the equator,
105 which brings more moisture to North China and increases the likelihood of precipitation.
106 Simultaneously, the positive phase of NAO can alter the atmospheric pressure in the North Atlantic,
107 influencing the atmospheric circulation over the Eurasian continent. This interaction between NAO
108 and ENSO synergistically regulates, to some extent, the distribution of precipitation in North China
109 (Guo et al., 2012).

110 It is evident that the synergistic effects of NAO and ENSO exert significant impacts on the
111 climate in China. However, the synergistic impacts of these two factors on the dust events in North
112 China remains unclear, and the underlying mechanisms and processes are yet to be elucidated.
113 Therefore, this study will examine the synergistic effects of NAO and ENSO on the dust weather in
114 North China. Moreover, given that the impacts of winter NAO and ENSO on the climate in China
115 is more pronounced (Zuo et al., 2016; Zhang et al., 2021b), our analysis will concentrate on the
116 influence of previous winter NAO and ENSO on the following spring dust, thereby providing a
117 scientific foundation for predicting dust events in China. The structure of this paper is as follows:
118 Section 2 outlines the datasets and methods employed in this study. Section 3 presents the analysis
119 and findings. Section 4 contains the summary and discussion.

120

121

122

123 **2. Datasets and methods**

124 **2.1 Datasets**

125 The dust dataset for the Modern-Era Retrospective Analysis for Research and Applications
126 Version 2 (MERRA-2) was obtained from NASA's Global Modeling and Assimilation Office
127 (GMAO), incorporating assimilated observations from both satellites and ground stations (Gelaro
128 et al., 2017). In this study, the Dust Column Mass Density of the MERRA-2 `tavg1_2d_aer_Nx`
129 product was utilized to represent the dust concentration with $0.5^\circ \times 0.625^\circ$ resolution. Previous
130 studies have demonstrated the accuracy and applicability of MERRA-2 reanalysis data for
131 simulating the spatiotemporal distribution characteristics of dust aerosol concentration in China. It
132 is reported that the result based on MERRA-2 are similar to those obtained from MODIS, OMPS,
133 CALIPSO, and Himawari-8 data (Kang et al., 2016; Wang et al., 2021). Additionally, the SST
134 dataset was derived from the Hadley Centre of the UK Met Office on a $1^\circ \times 1^\circ$ grid (Rayner et al.,
135 2003). The atmospheric reanalysis datasets employed herein were provided from the Fifth
136 Generation Reanalysis Version 5 (ERA5) of the European Centre for Medium-Range Weather
137 Forecasts (ECMWF) with a resolution of $0.25^\circ \times 0.25^\circ$ on 37 vertical levels (Hersbach et al., 2020),
138 including wind, geopotential height, and sea-level pressure, specific humidity, precipitation, and
139 vorticity. Considering the available period of all datasets, the common available period of 1979–
140 2022 was selected. The winter is defined as December-February (December-January-February, DJF),
141 with the winter of 1979 corresponding to the average of December in 1979, January and February
142 in 1980. The spring season is delineated as the average of March-May (March-April-May, MAM).
143 To enhance the investigation of the relationship between the NAO, ENSO, and dust activities over
144 North China, the linear trends of all variables were removed.

145 **2.2 Methods**

146 The NAO index (NAOI) used is following Li and Wang (2003), quantified by the difference in
147 the normalized monthly SLP regionally zonal averaged over the North Atlantic within 80°W - 30°E
148 between 35°N and 65°N . This definition effectively captures the large-scale circulation
149 characteristics associated with NAO, essentially measuring the intensity of zonal winds spanning
150 the entire North Atlantic. Note that the NAOI used in present work is well agree with that defined
151 by Hurrell (1995) and Jones (1997), with correlation coefficients of 0.96 and 0.94, respectively. And
152 that the result in the context is robust and would not be affect by the selection of NAOI. Furthermore,
153 ENSO is characterized by Niño3.4 index with SST anomalies averaged over 5°S - 5°N , 170°W -

154 120°W (Trenberth, 1997). In this study, we utilized the standardized indices of seasonal averages
 155 during 1980-2022, with values exceeding 0.5 standard deviations identified as anomalous years as
 156 shown in Table 1.

157 The memory effect of SST can be elucidated by the SST persistence component (SST_p), as
 158 delineated in equation (1) (Pan, 2005).

$$159 \quad SST_p = SST(t) * \frac{Cov[SST(t), SST(t+1)]}{Var[SST(t)]} \quad (1)$$

160 SST_p represents the memory effect of the previous SST (previous winter) on the following SST
 161 (spring), where $SST(t)$ and $SST(t+1)$ denote the previous winter SST and spring SST,
 162 respectively. $Cov[SST(t), SST(t+1)]$ denotes the covariance between the previous winter SST
 163 and spring SST, while $Var[SST(t)]$ signifies the variance of the previous winter SST.
 164 Consequently, the $Cov[SST(t), SST(t+1)]/Var[SST(t)]$ represents the connection between the
 165 SST variations in previous winter and spring. A greater value of SST_p indicates the variation of
 166 $SST(t+1)$ is more closely attached with the variation of $SST(t)$.

167 The T-N wave activity flux (WAF), formulated by Takaya and Nakamura (2001), represents a
 168 three-dimensional wave action flux that describes the energy dispersion characteristics of stationary
 169 Rossby waves, thereby reflecting the direction of Rossby wave energy dispersion. The WAF is
 170 suitable for application in mid-high latitude regions where the background circulation deviates from
 171 uniform zonality, as obviates the need for the assumption that the basic flow field must be a zonally
 172 averaged basic flow and can accommodate zonally non-uniform wind fields. The convergence and
 173 divergence characteristics of WAF reveal the source and dissipation areas of wave energy, with the
 174 transmission direction being interpretable as the direction of energy transport. The three-
 175 dimensional formulation of WAF is as follows:

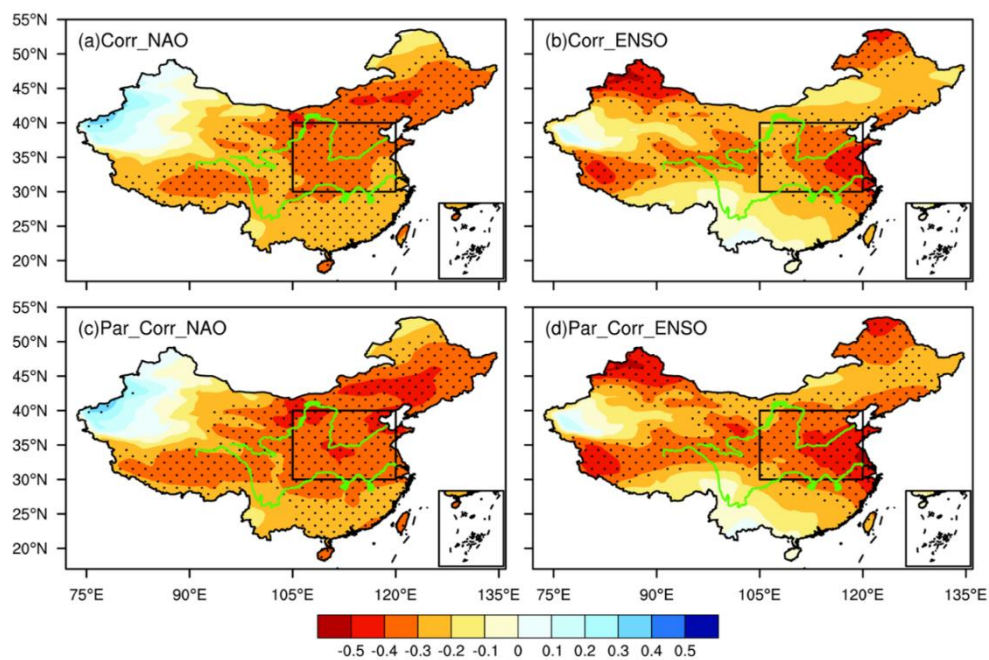
$$176 \quad W = \frac{pcos\varphi}{2|\mathbf{U}|} \cdot \left(\begin{array}{l} \frac{U}{a^2cos^2\varphi} \left[\left(\frac{\partial\psi'}{\partial\lambda} \right)^2 - \psi' \frac{\partial^2\psi'}{\partial\lambda^2} \right] + \frac{V}{a^2cos\varphi} \left[\frac{\partial\psi'}{\partial\lambda} \frac{\partial\psi'}{\partial\varphi} - \psi' \frac{\partial^2\psi'}{\partial\lambda\partial\varphi} \right] \\ \frac{U}{a^2cos\varphi} \left[\frac{\partial\psi'}{\partial\lambda} \frac{\partial\psi'}{\partial\varphi} - \psi' \frac{\partial^2\psi'}{\partial\lambda\partial\varphi} \right] + \frac{V}{a^2} \left[\left(\frac{\partial\psi'}{\partial\varphi} \right)^2 - \psi' \frac{\partial^2\psi'}{\partial\varphi^2} \right] \\ \frac{f_0^2}{N^2} \left\{ \frac{U}{acos\varphi} \left[\frac{\partial\psi'}{\partial\lambda} \frac{\partial\psi'}{\partial z} - \psi' \frac{\partial^2\psi'}{\partial\lambda\partial z} \right] + \frac{V}{a} \left[\frac{\partial\psi'}{\partial\varphi} \frac{\partial\psi'}{\partial z} - \psi' \frac{\partial^2\psi'}{\partial\varphi\partial z} \right] \right\} \end{array} \right) \quad (2)$$

177 In the expression, p , φ , λ , f_0 , and a represent the geopotential height, latitude, longitude,
 178 coriolis parameter, and Earth's radius, respectively. $\psi' = \Phi'/f$ (where Φ represents the
 179 geopotential) denotes the disturbance of the quasi-geostrophic stream function relative to the
 180 climatology. The basic flow field $\mathbf{U} = (U, V)$ denotes the climatic field, where U and V indicate
 181 the zonal and meridional velocities, respectively.

182 3. Results

183 3.1 Impacts of NAO and ENSO on the spring dust in North China

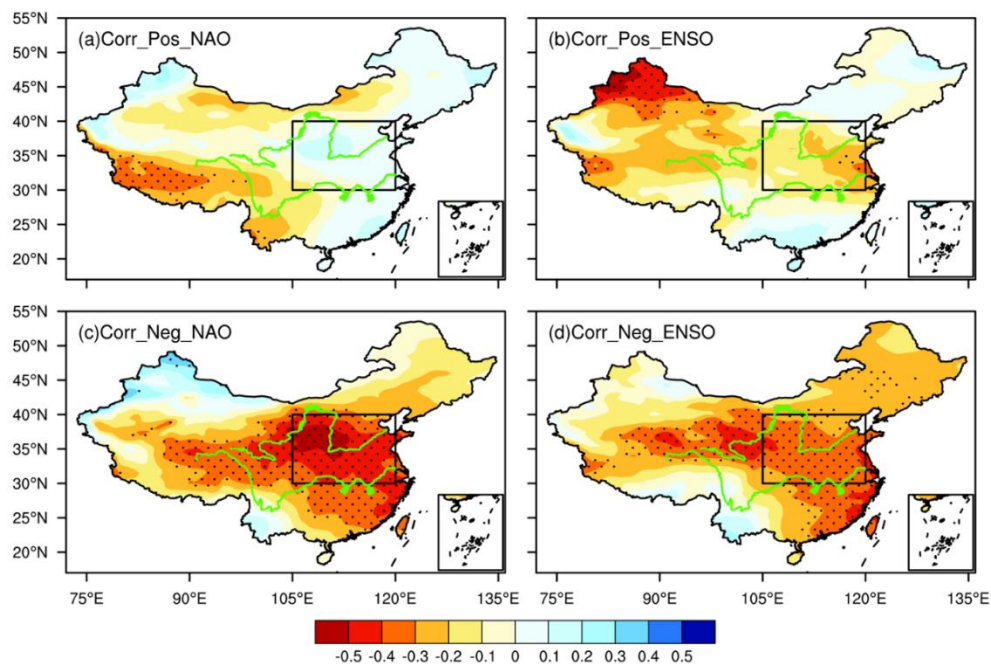
184 Previous studies have highlighted the significant impacts of NAO (e.g., Wu et al., 2009; Zheng
185 et al., 2016a; Wang et al., 2018) and ENSO (e.g., Zhao et al., 2016; Zhang et al., 2016; Feng et al.,
186 2020) on the climate anomalies over China. To investigate their effects on the spring dust, the
187 correlation between the previous winter NAO and ENSO and following spring dust concentrations
188 are examined (Figure 1). Significant negative correlations are observed over North China between
189 NAO and dust content. Similar relationship is seen in the ENSO case. This result indicates a lower
190 (higher) dust content is expected when NAO and ENSO are in the positive (negative) phases
191 (Figures 1a-b). Notably, North China is situated at the center of the maximum correlation, with
192 correlation coefficients of -0.36 and -0.35 between NAO and ENSO, respectively. Simultaneously,
193 considering the significant interaction between NAO and ENSO (López-Parages et al., 2015; Zhang
194 et al., 2015), to detect their independent effects on the dust content, the partial correlation between
195 NAO (ENSO) and dust content after removing the influence of the ENSO (NAO) are provided. The
196 results indicate that the significant correlation regions between dust concentrations and either NAO
197 or ENSO do not change significantly after removing the influence of the other. These findings
198 suggest a stable and significant connection between NAO and ENSO in the previous winter and the
199 dust content in North China (Figures 1c-d).



200

201 **Figure 1.** (a) Spatial distribution of correlation coefficients between the previous winter NAOI and
202 spring dust content. (b) As in (a), but with Niño3.4 index. (c) As in (a), but for the partial correlation
203 after removing the effect of ENSO. (d) As in (c), but after removing the effect of NAO. The black
204 box represents North China. Stippled areas are statistically significant at the 0.1 level.

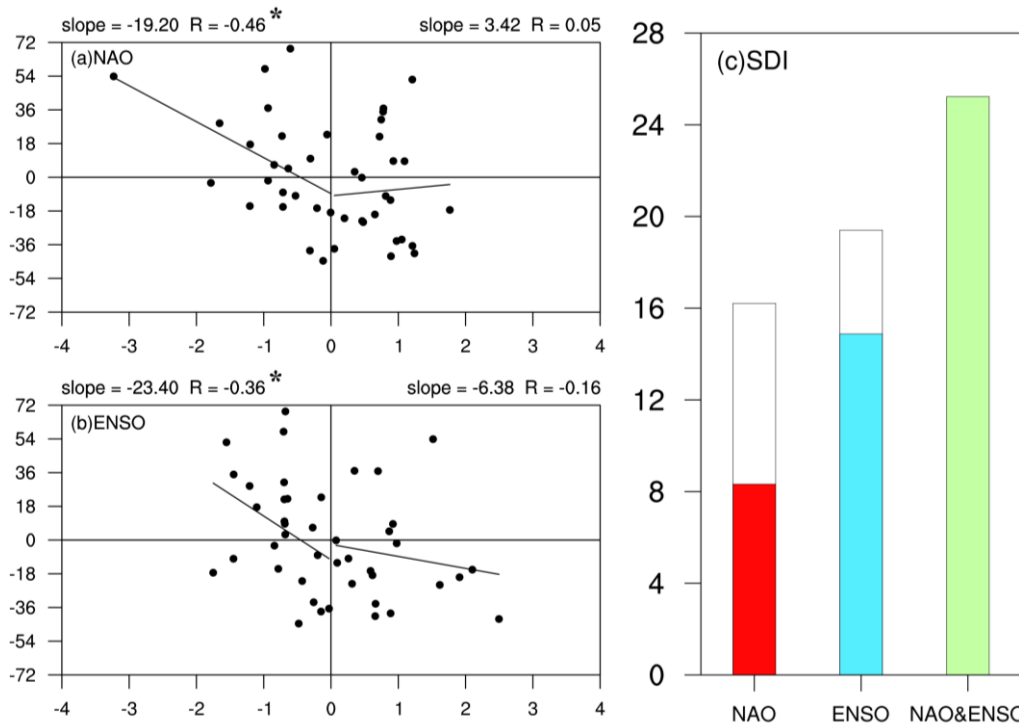
205 Previous studies have indicated that the development rate, intensity variations, and spatial
206 structure of NAO exhibit distinct asymmetric characteristics between different phases (Feldstein,
207 2003; Jia et al., 2007). Furthermore, the influence of NAO on the EAWM is more pronounced during
208 its negative phase (Sung et al., 2010). Similarly, both observational facts and model experiments
209 suggest that El Niño and La Niña, as the positive and negative phases of ENSO, are not simply
210 mirror images of each other. The SST anomalies in the tropical Pacific associated with ENSO exhibit
211 significant asymmetry in terms of meridional range (Zhang et al., 2009), amplitude (Su et al., 2010),
212 zonal propagation (McPhaden and Zhang, 2009), as well as climate impact (Feng and Li, 2011;
213 Yang et al., 2022b) under El Niño and La Niña conditions. Consequently, we further analyzed the
214 connection between NAO/ENSO and spring dust but in different phases. The results indicate that
215 the relationship between NAO/ENSO and dust in North China also exhibits significant asymmetry,
216 i.e., with weaker (stronger) correlations during positive (negative) phases of NAO and ENSO
217 (Figure 2), where significant correlations only appear in the negative phases of NAO and ENSO. To
218 comprehensively understand the effects of both NAO and ENSO on the dust activities in North
219 China, the areal average of spring dust content over North China was calculated, termed as the
220 spring dust index (SDI). Based on the scatter distribution of SDI under different phases of NAO and
221 ENSO, it is noted that the correlation coefficients between NAOI and SDI during the positive and
222 negative phases of NAO are -0.46 and -0.05, respectively, indicating that the significant influence
223 of NAO on the dust in North China mainly occurs during its negative phase (Figure 3a). Similarly,
224 the correlation distribution between the ENSO and SDI also shows that the influence of ENSO is
225 more pronounced during its negative phase (Figure 3b). These results indicate that the impacts of
226 previous winter NAO and ENSO on the spring dust content in North China exhibit asymmetrical
227 characteristics, significant effects mainly manifested during their negative phases.



228

229 **Figure 2.** Spatial distribution of correlation coefficients between (a) positive and (c) negative NAOI
 230 values and dust content. (b) and (d) As in (a) and (b), respectively, but for the Niño3.4 index.
 231 Stippled areas are statistically significant at the 0.2 level.

232 The synergistic effects of climate variabilities from mid-high latitudes and tropics are pivotal
 233 mechanisms affecting the weather and climate in East Asia (Feng et al., 2019; Li et al., 2019).
 234 Correspondingly, we will examine whether the negative phases of previous winter NAO and ENSO
 235 exert synergistic effects on the following spring dust content in North China. As shown in Figure
 236 3c, when the NAO is in its negative phase, including alone occurrence and in conjunction with
 237 negative phase of ENSO, the anomalous values of dust content is $8.32 \text{ mg}\cdot\text{m}^{-2}$ and $16.21 \text{ mg}\cdot\text{m}^{-2}$,
 238 respectively. Similarly, the anomalous dust content is $14.88 \text{ mg}\cdot\text{m}^{-2}$ and $19.40 \text{ mg}\cdot\text{m}^{-2}$ for the case
 239 of ENSO. When the NAO and ENSO both are in negative phases, the value of dust anomaly (25.23
 240 $\text{mg}\cdot\text{m}^{-2}$) is much greater than the situation when one of them is in the negative phase. That is the
 241 negative phases of previous winter NAO and ENSO demonstrate synergistic effects on the spring
 242 dust activities in North China. To enhance the robustness of statistical analysis, we aim to select
 243 representative samples. Consequently, we focus on cases when both the NAO and ENSO are in
 244 negative phases. Therefore, three categories, i.e., only the NAO (ENSO) is in its negative phase,
 245 and both NAO and ENSO are in the negative phases (Table 1) are discussed in the context to
 246 elucidate the relevant process of the synergistic effects of NAO and ENSO on the dust content over
 247 North China.



248

249 **Figure 3.** Scatterplots of the spring dust content in North China against previous winter (a) NAOI
 250 and (b) Niño3.4 index. Also shown are lines of best fit for positive and negative NAO/Niño3.4 index
 251 values and correlation coefficients (R), slope (slope), * indicates significant at the 0.2 level. (c)
 252 Spring dust content over North China during the negative NAO, negative ENSO phases, and
 253 concurrent negative phases of NAO and ENSO (unit: $\text{mg} \cdot \text{m}^{-2}$). Transparent bars represent negative
 254 phases of the NAO and ENSO, filled bars indicate negative phases of the NAO and ENSO occurring
 255 separately and co-occurring.

256 **Table 1.** The events of NAO and ENSO classified by three categories during period 1980-2022

	Years	Numbers
NAO ⁻	1980,1982,1985,1986,1987,1996,1998,2001, 2003,2004,2006,2010,2011,2013,2021	15
ENSO ⁻	1984,1985,1986,1989,1996,1999,2000,2001, 2006,2008,2009,2011,2012,2018,2021,2022	16
NAO ⁻ & ENSO ⁻	1985,1986,1996,2001,2006,2011,2021	7

257 3.2 Impacts of NAO and ENSO on the environmental variables

258 To examine the anomalous characteristics associated with NAO and ENSO, the circulation
 259 anomalies in their solo negative phases, as well as in their co-occur negative phases (Table 1) are
 260 analyzed. In the upper troposphere (200 hPa), the zonal wind is strengthened over the northwest of
 261 China and Mongolia during the negative NAO phase (Figure 4a), with evident positive anomalies
 262 centered around Mongolia, reaching a maximum value of $+1.5 \text{ m} \cdot \text{s}^{-1}$. In the case of negative ENSO
 263 phase, the upper-level zonal wind also shows an intensification over the northwest region of China

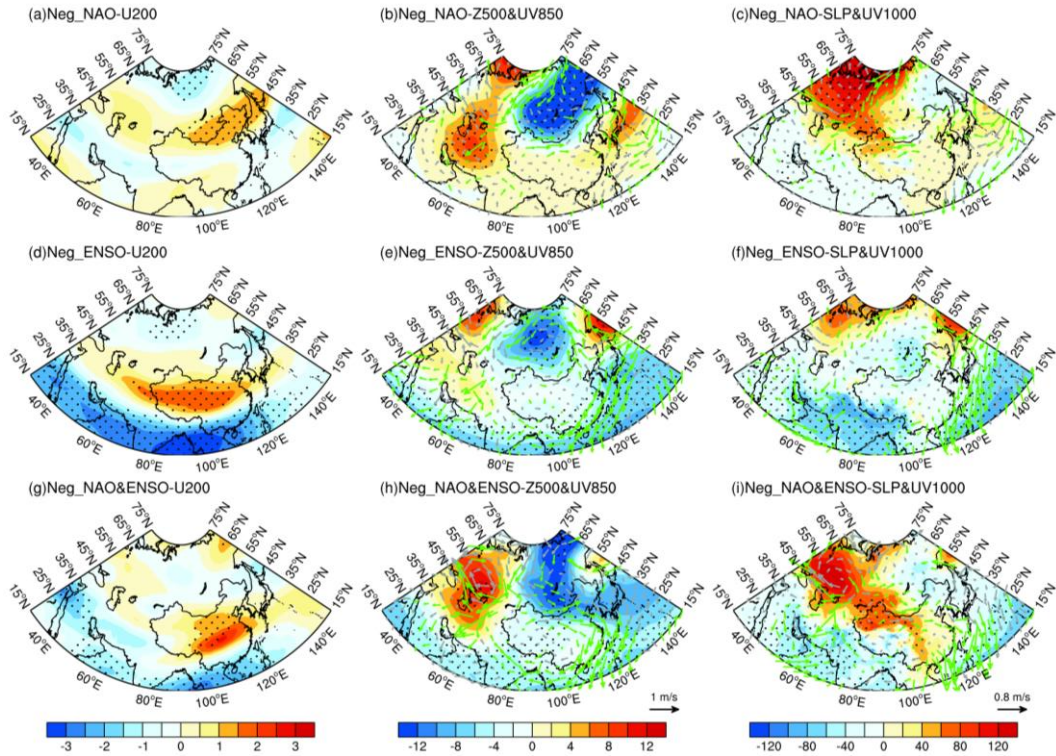
264 and Mongolia, with a maximum value of $+2 \text{ m}\cdot\text{s}^{-1}$ (Figure 4d). The intensification of upper-level
265 zonal wind boosts the upper-level momentum, which is subsequently transferred downward to the
266 mid-lower troposphere through vertical circulation (Wu et al., 2016; Li et al., 2023), causing windy
267 weather in the surface dust source regions, facilitating dust lifting and transport activities, thereby
268 promoting the occurrence of dust weather in the downstream North China. When both the NAO and
269 ENSO are in their negative phases, the main positive anomaly center appears over North China,
270 reaching a maximum value of $+3 \text{ m}\cdot\text{s}^{-1}$, which is stronger than the situation in either the NAO or
271 ENSO. This result implies the synergistic effects of NAO and ENSO on the upper-level zonal wind,
272 facilitating an enhanced transport of dust from its source regions to North China, consequently
273 triggering the onset of dust weather conditions in North China (Figure 4g).

274 Subsequent analysis delved into the anomalous distribution of the circulation field in the mid
275 and lower troposphere. In the negative NAO phase, a pronounced 'trough-ridge' anomaly pattern
276 emerges in the mid-latitude region, characterized by a trough in Siberia and a ridge in the Middle
277 East, with their anomalous intensities reaching -12 gpm and $+10 \text{ gpm}$, respectively (Figure 4b). This
278 atmospheric configuration fosters a dominant meridional circulation in the mid-high latitude region,
279 thereby facilitating the enhanced transport of cold air from the north. Such a southward incursion
280 of cold air serves to strengthen the surface wind speeds, and to promote the uplift and transport of
281 dust from the source regions. In the negative ENSO phase, although the mid-latitude region exhibits
282 a similar trough-ridge pattern, more pronounced circulation anomalies are observed over the WNP.
283 At this time, the region is predominantly under the influence of northeasterly winds on its western
284 flank, manifesting a cyclonic circulation anomaly (Figure 4e), consistent with previous research
285 results (Ke et al., 2023). This abnormal circulation will hinder the northward transport of warm and
286 moist air from the South China Sea and the Bay of Bengal, diminishing the likelihood of interactions
287 with cold air from the north, thus reducing the possibility for the formation of stationary fronts and
288 precipitation. The decrease in precipitation weakens the wet deposition effect (Zheng et al., 2016b;
289 Huang et al., 2021), favoring the occurrence of dust weather in the region. When both the NAO and
290 ENSO are simultaneously in their negative phases, the meridional circulation in the mid-latitude
291 region is notably enhanced, with the maximum anomalies of the trough and ridge reaching -12 gpm
292 and $+12 \text{ gpm}$, respectively (Figure 4h). Furthermore, the southward shift of the trough-ridge pattern
293 leads to a more significant increase in wind speed in the upstream dust source regions of North
294 China, providing a more substantial source of dust for North China. Meanwhile, the presence of a
295 cyclonic circulation anomaly over the WNP reduces the transport of warm and moist air from the

296 south, which is unfavorable for precipitation, thereby lowering the wet deposition effect on dust and
297 further favoring the onset and intensification of dust activities in North China.

298 As for the SLP, significant positive SLP anomalies appear in Eastern Europe and the Russian
299 during negative NAO phase, indicative of an intensified Siberian High (SH), which extends
300 southward to the dust source regions upstream of North China (Figure 4c). The intensification of
301 the SH typically accompanied with strong northerlies and dry conditions, favoring for the transport
302 of dust, thereby supplying abundant material sources for dust activities in North China. In the
303 negative ENSO phase, although the high-latitude region exhibits a weaker SH signal, similar to the
304 ENSO influence on the circulation pattern in the middle and lower troposphere, more significant
305 circulation anomalies occur over the WNP. This cyclonic circulation anomaly inhibits the northward
306 transport of warm and moist air from the south, leading to poorer precipitation conditions in North
307 China (Figure 4f). When both the NAO and ENSO are in their negative phases, the strength and
308 influence extent of the SH are more pronounced compared to that when the NAO sole is in negative
309 phase. Besides, there persists a cyclonic circulation anomaly over the WNP, which is conducive to
310 the occurrence of dust events in North China (Figure 4i).

311 The results suggest that when both the NAO and ENSO are in their negative phases, synergistic
312 effects emerge, rendering the atmospheric circulation in the troposphere more conducive to the
313 occurrence of dust events in North China. The synergistic effects may be due to the superposition
314 and interaction of various atmospheric levels and regional characteristics modulated by the NAO
315 and ENSO, thereby forming more favorable circulation conditions for dust activities in North China.

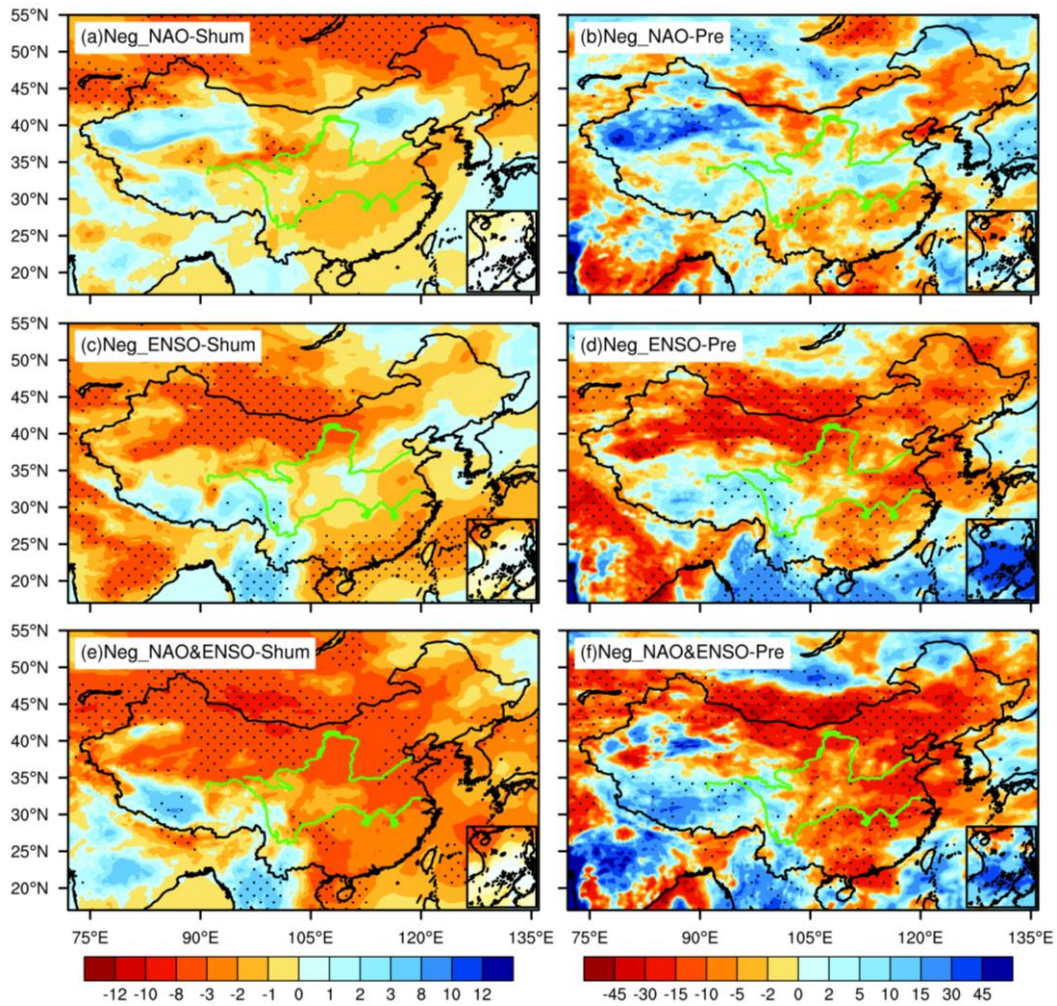


316

317 **Figure 4.** Upper, (a) 200 hPa zonal wind anomalies (shading, unit: $\text{m}\cdot\text{s}^{-1}$), (b) 500 hPa geopotential
 318 height (shading, unit: gpm) and 850 hPa wind field anomalies (arrows, unit: $\text{m}\cdot\text{s}^{-1}$), (c) sea-level
 319 pressure (shading, unit: Pa) and 1000 hPa wind field anomalies (arrows, unit: $\text{m}\cdot\text{s}^{-1}$) during the
 320 negative NAO phases. Middle-Lower, as in the upper, but during the negative ENSO phases and
 321 concurrent negative phases of NAO and ENSO, respectively. Stippled areas and green arrows are
 322 statistically significant at the 0.2 level.

323 Dust activities are multifaceted phenomenon related to large-scale circulation patterns, and
 324 significantly influenced by local surface conditions and meteorological processes. It is found that
 325 surface properties and local meteorological factors play a role in the initiation, development, and
 326 dissipation of dust activities (e.g., Liu et al., 2004; Yao et al., 2021; Huang et al., 2021). In particular,
 327 humidity and precipitation play decisive role in determining the frequency and intensity of dust
 328 activities (Prospero et al., 1987; Kim and Choi, 2015). Low humidity leads to drier soil conditions
 329 in the dust source regions, reducing the cohesion between soil particles and facilitating dust lifting
 330 and transport activities (Csavina et al., 2014), and vice versa. Similarly, the amount of precipitation
 331 directly affects the wet deposition process of dust. Low precipitation weakens the wet deposition,
 332 resulting in relatively stronger dust activities (Zheng et al., 2016b). Therefore, we further analyzed
 333 their potential impacts on the humidity and precipitation. When the NAO is in its negative phase,
 334 humidity in the spring dust source regions and North China generally reduced, particularly in areas
 335 near the dust source regions, indicating that these areas are conducive to dust transport and prone to
 336 causing dust weather in North China (Figure 5a). As for the precipitation, there is more spring

337 precipitation in the northwest region of China, while precipitation in the Mongolia and the North
338 China is relatively less (Figure 5b). In the negative ENSO phase, the variation in humidity is similar
339 to that during the negative NAO phase, but with a greater amplitude (Figure 5c), indicating that
340 ENSO has a stronger impact on the humidity conditions in North China. Moreover, the precipitation
341 shows a significant abnormal decrease over Mongolia and North China, which is highly conducive
342 to dust activities and the generation of dust weather (Figure 5d). When both the NAO and ENSO
343 are in the negative phases, the humidity anomalies in the dust source regions and North China are
344 more intense than the individual factor (Figure 5e). The variation in precipitation are similar to those
345 in humidity, the reduction in precipitation in the dust source regions and North China exceeds the
346 sole role (Figure 5f). The aforementioned analysis indicates that NAO and ENSO can modulate
347 humidity and precipitation, ultimately affecting dust weather. During the negative NAO phase, the
348 diminished atmospheric pressure gradient in the mid-high latitude regions of North Atlantic leads
349 to the intensification and southward shift of the SH (Zhou et al., 2023), accompanied by strong wind,
350 making drier and conducive to dust lifting and transport in the dust source regions. In the negative
351 ENSO phase, the upper atmosphere over the WNP is dominated by significant negative anomalies
352 in geopotential height and northeasterly winds (Zhang et al., 2015), reducing moist transport. When
353 the NAO and ENSO both are in negative phases, their regulation of atmospheric circulation
354 produces synergistic effects, further influencing the variations of humidity and precipitation, thereby
355 promoting the occurrence and development of dust activities in North China.



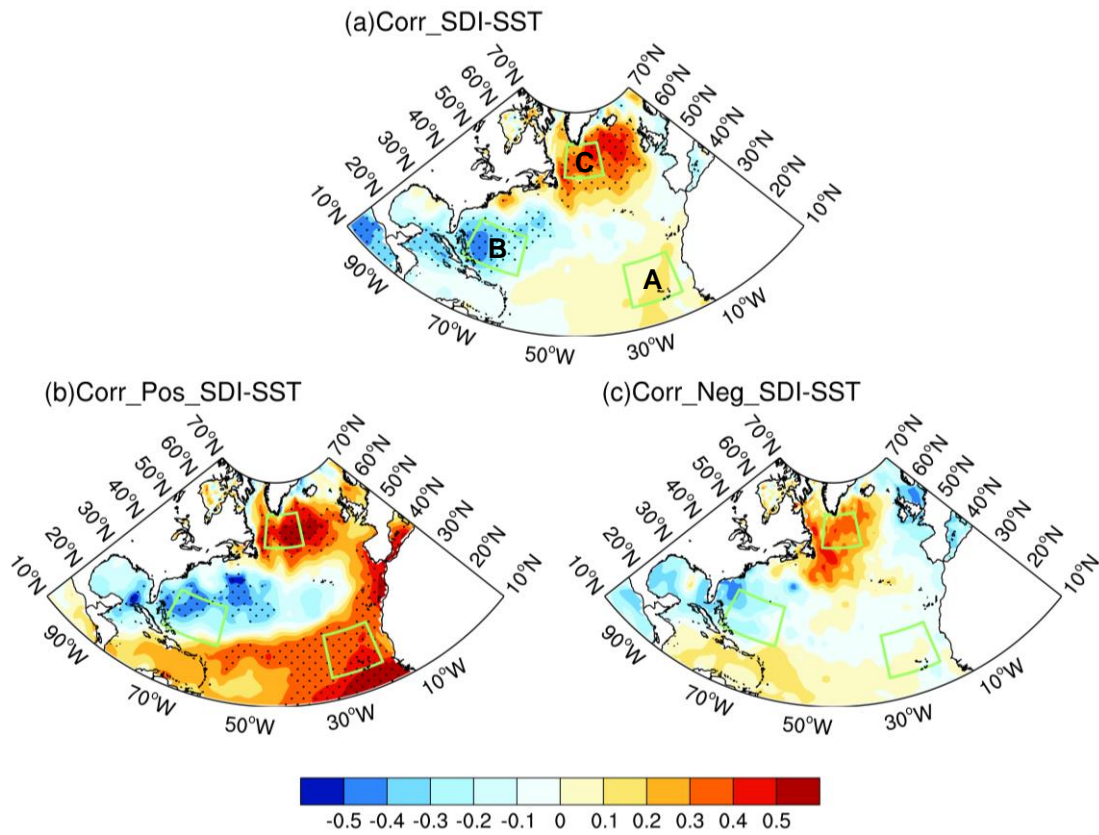
356

357 **Figure 5.** Upper, composite percentage anomalies of (a) humidity and (b) precipitation during
 358 negative NAO phases. Middle-Lower, as in the upper, but during negative ENSO phases and
 359 concurrent negative phases of NAO and ENSO, respectively. Stippled areas are statistically
 360 significant at the 0.2 level.

361 **3.3 Physical Mechanisms of the NAO and ENSO on the dust weather**

362 The above results demonstrated that the previous winter NAO and ENSO exert significant
 363 impacts on the spring dust activities in North China. Consequently, an examination of the underlying
 364 physical mechanisms is warranted. Given the relatively short memory of NAO as an atmospheric
 365 phenomenon, we will employ the concept of ocean-atmosphere coupling bridge to elucidate the
 366 involved processes. The previous ENSO signal can alter the atmospheric circulation over the WNP
 367 through the persistent impact of SST, thereby significantly affecting subsequent weather and climate
 368 in China (e.g., Wu et al., 2017; Kim and Kug, 2018; Jiang et al., 2019). The tripole configuration of
 369 SST is the leading mode of SST variation in the North Atlantic, and its variabilities are closely
 370 associated with the NAO (Wu et al., 2009; Figure 7a), which allows the previous NAO signal to

371 exert a long-term influence on the subsequent weather and climate in China (e.g., Chen et al., 2020;
 372 Wu and Chen, 2020; Song et al., 2022). The variation of SDI is linked with an anomalous tripole
 373 SST in the North Atlantic (Figure 6a), paralleling with the SST anomalies accompanied with the
 374 negative phase of NAO. Therefore, the North Atlantic tripole index (NATI) is further delineated
 375 (Equations 3-6), as well as the relationships among the NAOI, NATI, and SDI are explored. The
 376 correlation analysis between the high and low years of SDI and NATI reveals a pronounced
 377 difference, indicating an asymmetric correlation (Figures 6b-c). Specifically, the significant
 378 relationship between SDI and NATI only existed in the positive SDI years, implying the occurrence
 379 of NATI would be connected with more dust weather over North China.



380

381 **Figure 6.** (a) Spatial distribution of the correlation coefficients between the spring SDI and
 382 simultaneous SST. (b)-(c) As in (a), but for the positive and negative phase of SDI. Stippled areas
 383 are statistically significant at the 0.2 level.

384
$$\text{SST}_A = [15-25^\circ\text{N}, 32-20^\circ\text{W}] \quad (3)$$

385
$$\text{SST}_B = [22-32^\circ\text{N}, 75-60^\circ\text{W}] \quad (4)$$

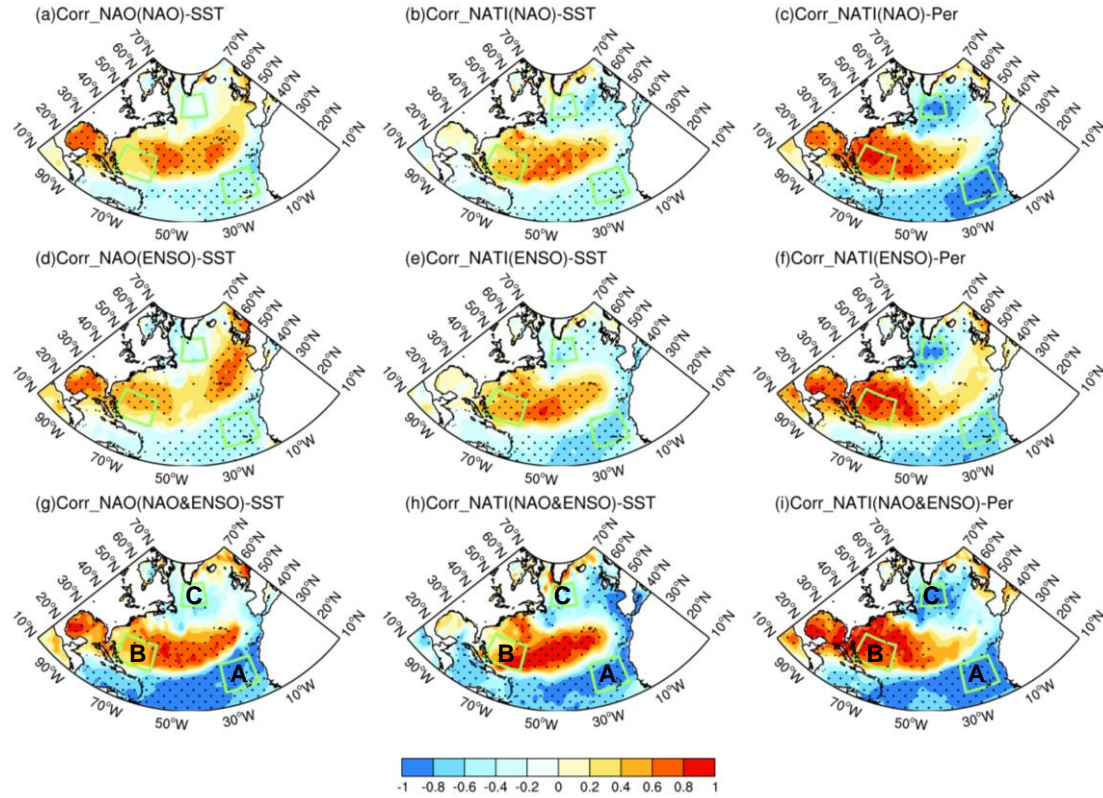
386
$$\text{SST}_C = [50-60^\circ\text{N}, 50-32^\circ\text{W}] \quad (5)$$

387
$$\text{NATI} = \text{SST}_B - \frac{1}{2}(\text{SST}_A + \text{SST}_C) \quad (6)$$

388 Subsequent analyses delved into the association between the previous winter NAO and the

389 North Atlantic SST. It is seen that the correlation coefficients between the negative (positive) NAOI
390 and NATI are 0.41(-0.09) (figures not shown), indicating that the influence of previous winter NAO
391 on the following spring NATI only manifest during its negative phase. This elucidates the reason
392 why the significant impact of NAO on the dust activities in North China only existed during its
393 negative phase. In the negative NAO phase, there is a notable correlation between the previous
394 winter NATI and the spring SST and SST_p (Figures 7b-c), indicating that the previous winter NATI
395 can persist to spring, in which the self-persistence of SST playing a crucial role. Similar findings
396 are observed during the negative phase of ENSO (Figures 7d-f) and when both the NAO and ENSO
397 occur simultaneously (Figures 7g-i).

398 The correlation between the previous winter NAO and North Atlantic SST reveals that in the
399 NAO negative phase (Figure 7a), the variation of NAO is linked with an anomalous tripole SST
400 pattern in the North Atlantic. Meanwhile, similar findings are observed when negative ENSO events
401 occur (Figure 7d). This suggests that there may be a positive feedback occurred between NAO and
402 North Atlantic SST during negative ENSO phase. When both the NAO and ENSO are in the
403 negative phases, the anomalous tripole SST pattern is more pronounced (Figure 7g). This further
404 elucidates that ENSO exerts a promoting effect on strengthening the connection between the
405 negative NAO and NATI, thereby providing an explanation for the synergistic effects of the NAO
406 and ENSO on the dust weather in North China. Additionally, the correlation coefficients between
407 the NAOI and NATI under different scenarios can illustrate the synergistic influence of the NAO
408 and ENSO on the persistence of SST anomalies (Table 2). Specifically, when the negative phase of
409 NAO and ENSO occur together, the correlation coefficients between the NAOI and NATI are greater
410 than those influenced by a single factor alone (Table 2). The impacts of previous winter NAO on
411 the spring dust activities over North China are mainly include 1) The previous winter NAO would
412 stimulate the anomalous NAT SST pattern; 2) The NAT can last from previous winter to the
413 following spring due to the thermal persistence of the SST; 3) The spring NAT plays significant
414 modulation on the circulation pattern over North China through teleconnection wave trains, which
415 ultimately affects the spring dust activities over North China. It is seen from Table 2 that although
416 in the case of ENSO- phase and NAO- & ENSO- phase, the correlation coefficients of previous
417 winter NATI and spring NATI are same. However, the correlations between the NAOI and NATI is
418 higher during NAO- & ENSO- phase (0.66) than ENSO- phase (0.52), highlighting the significant
419 role of NAO on the NAT in the case of NAO- & ENSO- phase. The above discussion illustrates the
420 synergistic effect of NAO and ENSO on the dust activities over North China.



421

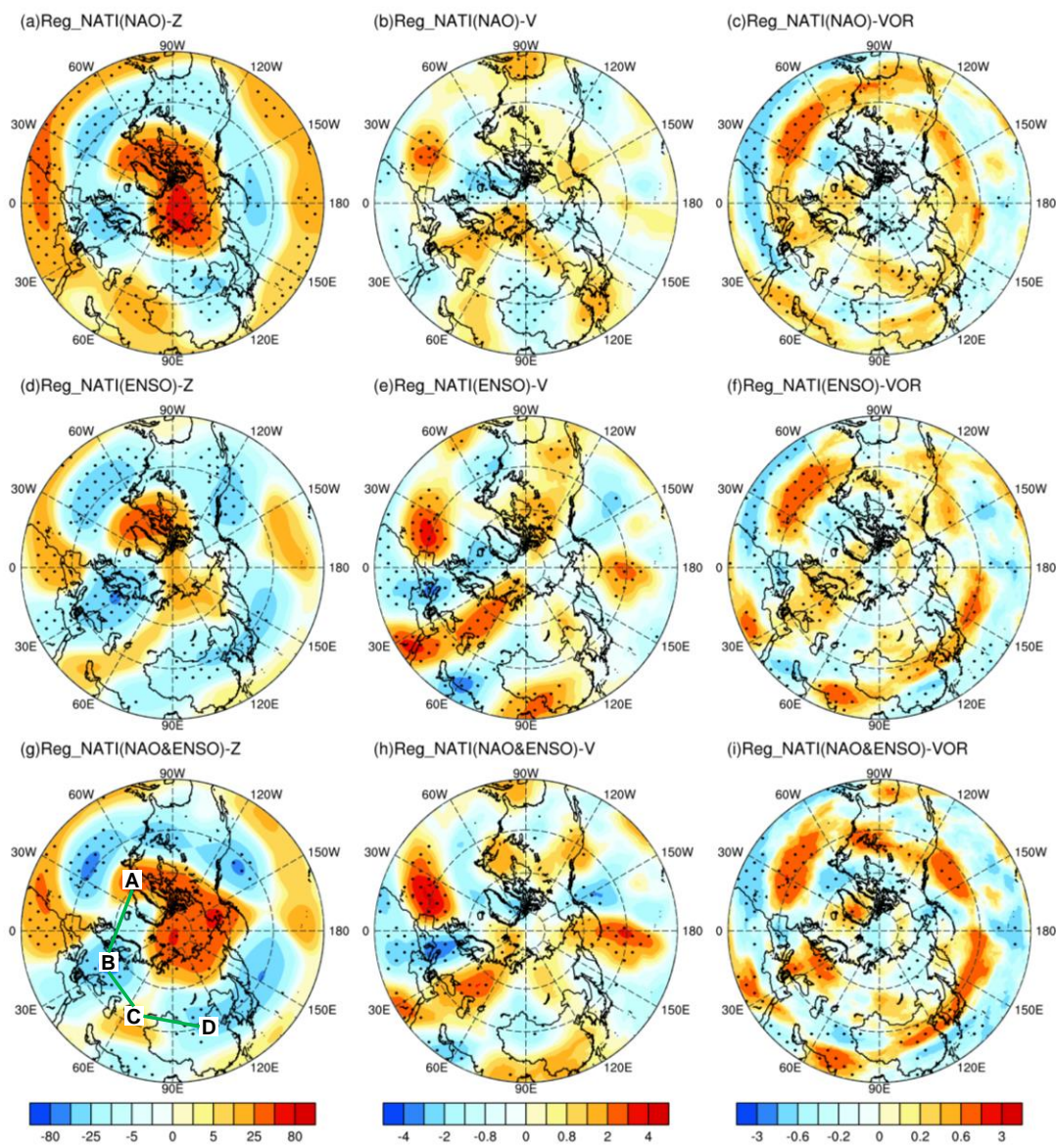
422 **Figure 7.** Upper, correlation distributions of the (a) winter NAOI with winter SST, (b) winter NATI
 423 with spring SST, and (c) winter NATI with SST_p during negative NAO phases. Middle-Lower, as
 424 in the upper, but during the negative ENSO phases and concurrent negative phases of NAO and
 425 ENSO, respectively. Stippled areas are statistically significant at the 0.2 level.

426 **Table 2.** Correlation coefficients between the NAOI and NATI in three different categories. *
 427 indicates significant at the 0.1 level.

	DJF_NAO & DJF_NATI	DJF_NATI & MAM_NATI
NAO ⁻ phase	0.41*	0.51*
ENSO ⁻ phase	0.52*	0.69*
NAO ⁻ & ENSO ⁻ phase	0.66*	0.69*

428 The NAO preserves its anomalous signal within the tripole SST during the previous winter,
 429 and releases the signal in the following spring. Given the distance across the entire Eurasian
 430 continent between the North Atlantic and North China, the role of teleconnection wave trains is
 431 particularly important in influencing dust activities over North China. Figure 8a illustrates the
 432 geopotential height field at 200 hPa regressed onto the spring NATI during the negative phase of
 433 NAO. This reveals a pronounced north-south reversed dipole pattern in the North Atlantic, i.e.,
 434 negative over Azores and positive over Iceland, representing a typical negative NAO structure (e.g.,
 435 Wallace and Gutzler, 1981; Hurrell, 1995; Li and Wang, 2003). Meanwhile, a positive-negative-
 436 positive teleconnection wave train structure centered around eastern Europe, Middle East, and North

437 China is observed, suggesting that the disturbance energy propagates downstream from the North
 438 Atlantic through waveguide effects, leading to an anticyclonic circulation anomaly in North China.
 439 Similar teleconnection wave-train propagation characteristics are also observed in the 200 hPa
 440 meridional wind and vorticity fields (Figure 8b, c). During the negative phase of ENSO, modulated
 441 by the NATI, analogous teleconnection structures are also seen in the circulation field (Figure 8d-
 442 f). Notably, when the NAO and ENSO are both in their negative phases, the teleconnection structure
 443 reflected in the circulation field is more pronounced than when only one factor is dominated (Figure
 444 8g-i), confirming the synergistic effects of both factors on the circulation processes affecting dust
 445 activities in North China.

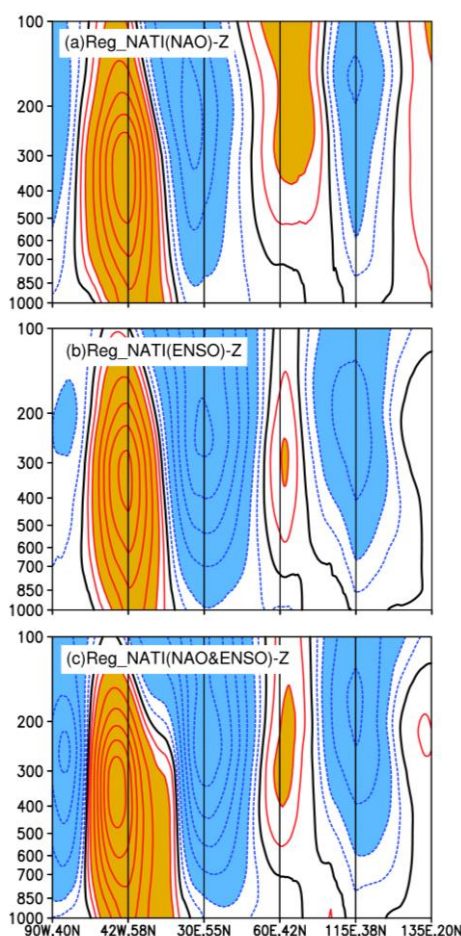


446

447 **Figure 8.** Upper, regression distribution of spring NATI against the spring (a) geopotential height
 448 (unit: gpm), (b) meridional wind (unit: $\text{m}\cdot\text{s}^{-1}$), and (c) vorticity (unit: $10^{-5}\cdot\text{m}\cdot\text{s}^{-1}$) at 200 hPa during

449 the negative NAO phase. Middle-lower, as in the upper, but during the negative ENSO phases and
450 concurrent negative phases of NAO and ENSO, respectively. Regression fields multiplied by -1.
451 Stippled areas are statistically significant at the 0.2 level.

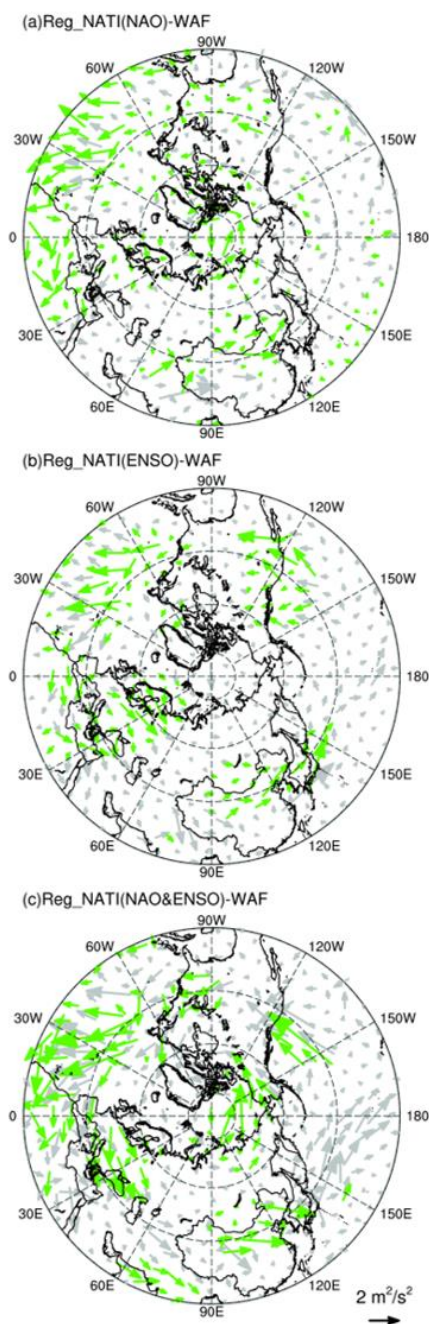
452 In order to further examine the impact mechanisms of the NAO and ENSO on the spring dust
453 activities in North China, based on the propagation characteristics of the teleconnection wave train
454 shown in Figure 8, the distribution of cross-section of the geopotential height field is presented
455 (Figure 9). When both the NAO and ENSO are in their negative phases, the NATI anomalies
456 correspond to the teleconnection wave train extending from the upper to lower troposphere, which
457 is specifically characterized by a positive-negative-positive tripole pattern. This wave train
458 propagates from the North Atlantic, traversing eastern Europe and Middle East, and ultimately
459 influencing circulation processes associated with the dust weather over North China. Furthermore,
460 the analysis of cross-section at different levels of the troposphere reveals that under the negative
461 phases of NAO and ENSO, the teleconnection wave train excited by the NATI exhibits quasi-
462 barotropic features, with this anomalous structure being primarily concentrated in the middle-upper
463 troposphere. When the NAO and ENSO are simultaneously in their negative phases, the intensity
464 and scope of the teleconnection wave train are significantly enhanced and expanded compared to
465 the influence of a single factor (Figure 9c), demonstrating synergistic effects.



466

467 **Figure 9.** Vertical section of regression of spring NATI against the geopotential height along the
 468 solid line labeled A (42°W, 58°N), B (30°E, 55°N), C (60°E, 42°N), and D (115°E, 38°N) in Figure
 469 8g for (a) negative NAO phase in the previous winter. Panels (b)-(c) as in (a), but during the negative
 470 ENSO phases and concurrent negative phases of NAO and ENSO, respectively (unit: gpm).
 471 Regression fields have multiplied by -1. Shading indicates the absolute value is greater than 10 gpm.

472 To provide a more comprehensive analysis of the transport process of disturbance energy in
 473 the atmosphere, the horizontal distribution of the WAF associated with spring NATI variations is
 474 further examined. Under the scenario that either the NAO or ENSO is in their negative phases, WAF
 475 can be clearly observed to originate from the North Atlantic, traverse the Eurasian continent, and
 476 extend to the North China (Figures 10a-b). When both factors occur simultaneously, not only is the
 477 transport intensity of WAF enhanced, but its impact range on the dust weather in North China is also
 478 broadened (Figure 10c). Through the analysis of teleconnection wave trains and WAF, it is
 479 determined that the synergistic effects not only enhance the disturbance intensity in the atmosphere
 480 but also expand impact range, thereby promoting the occurrence and development of spring dust
 481 weather in North China. The enhancement and expansion of atmospheric disturbances may be
 482 related to large-scale circulation anomalies and local climate condition changes induced by the
 483 synergistic effects of the NAO and ENSO, which in turn affect the transport and deposition



485

486 **Figure 10.** Upper, regression distribution of spring NATI against the T-N wave activity flux (a)
 487 during negative NAO phase. Middle-lower, as in upper, but during the negative ENSO phases and
 488 concurrent negative phases of NAO and ENSO, respectively (units: m²·s⁻²). Regression fields have
 489 multiplied by -1. Green arrows are statistically significant at the 0.2 level.

490 **4. Conclusions and discussions**

491 The NAO and ENSO exert significant impacts on climate variability in China (e.g., Zhang et
 492 al., 2016; Wang et al., 2018; Feng et al., 2020). Although North China is not the primary dust source,

493 dusty disasters are notably active in this region during spring. This study highlights that the previous
494 winter NAO and ENSO exert essential influences on the following spring dust activities in North
495 China. Their impacts are asymmetric, manifesting only when both are in their negative phases.
496 Furthermore, the results indicate that NAO and ENSO in the negative phase have synergistic effects
497 on the spring dust activities in North China, promoting dust activities and with greater impacts than
498 their sole effect.

499 Under the regulatory influence of the negative phases of NAO and ENSO, the atmospheric
500 circulation in the troposphere from the lower to upper layers exhibits anomalies, including variations
501 in the upper-level zonal winds, mid-latitude trough-ridge systems, circulation over the WNP, and
502 SH at the SLP. These variations promote the occurrence and development of dust weather in North
503 China. Simultaneously, accompanying anomalies in the atmospheric circulation pattern also affect
504 local meteorological factors, including humidity and precipitation, which in turn show impacts on
505 the dust activities in North China. Notably, when both the NAO and ENSO are in their negative
506 phases, synergistic effects occur, making the anomalies in atmospheric circulation from the lower
507 to upper layers, as well as variations in humidity and precipitation, more conducive to the occurrence
508 of dust events in North China. The impact of NAO on the underlying SST pattern is predominantly
509 observed during its negative phase, elucidating why the NAO significantly influences dust activities
510 in North China only during its negative phase. Furthermore, when both the NAO and ENSO
511 simultaneously manifest in their negative phases, the teleconnection wave trains and WAF
512 stimulated from the North Atlantic are more intense, thereby more effectively influencing dust
513 activities in North China, indicating the synergistic effects of the two variabilities on the dust
514 activities over North China.

515 In the process where the previous winter NAO and ENSO affect the following spring dust
516 activities in North China, the persistence of anomalous NAT over North Atlantic plays an important
517 role. The previous winter NAO stores its signal in the NAT (Wu et al., 2009). Due to the persistence
518 of SST, the anomalous NAT can last from winter to spring (e.g., Wu et al., 2012; Zhang et al., 2021a;
519 Li et al., 2023). In spring, NAT regulates the circulation pattern in North China through
520 teleconnection wave trains, ultimately affecting the dust activities over North China. The signal of
521 previous winter ENSO can persist into spring, due to the persistence of SST, and it affects the dust
522 activities in North China through two pathways: i.e., directly influencing the dust activities in North
523 China by affecting the circulation anomalies over the WNP, and playing a facilitating role in the
524 process where the NAO excites NAT, thereby affecting the dust activities in North China. This

525 provides a plausible explanation why the previous winter NAO and ENSO exert synergistic effects
526 on the following spring dust activities in North China.

527 This study investigated the impacts of NAO and ENSO on the dust activities in North China
528 and the involved physical processes, indicating the one season ahead signals provide as the useful
529 predictors for the spring dust activities in North China. Future work will focus on developing a
530 forecast model using the NAO and ENSO as predictors and validating its prediction effectiveness.
531 Additionally, as previous studies have highlighted strong interdecadal variations are existed in both
532 NAO and ENSO (Woollings et al., 2015; Wang et al., 2023), it is of interest to further detect whether
533 the synergistic effects of NAO and ENSO on the dusty activity over North China experience
534 interdecadal variations. However, due to the availability of dataset, the potential impacts of the
535 interdecadal variability of the NAO and ENSO on dust activities have not been discussed in this
536 study. Simultaneously, as reported that the state-of-art models can reproduce the individual impact
537 of NAO and ENSO on the dust activities in North China (Yang et al., 2022a), whether their
538 synergistic effects on the dust weather could be well simulated, requiring further researches.
539 Additionally, previous studies have indicated that the uncertainty in ENSO variability is likely to
540 increase under the background of global warming (Cai et al., 2021; Chen et al., 2024). Therefore, it
541 is crucial to investigate the future changes in the NAO, as well as future change of its synergistic
542 effects with the ENSO on the dust weather, to better understand the plausible trends of future dust
543 activities in North China.

544

545 **Code and data availability.** The MERRA-2 dust aerosol concentrations dataset can be downloaded
546 from <https://disc.gsfc.nasa.gov/datasets?project=MERRA-2> (last access: 28 March 2024). The
547 atmospheric reanalysis datasets, including the wind field, geopotential height field, and sea level
548 pressure field can be downloaded from
549 <https://cds.climate.copernicus.eu/#!/search?text=ERA5&type=dataset> (last access: 12 June 2024).
550 The oceanic reanalysis data can be downloaded from <https://www.metoffice.gov.uk/hadobs/hadisst>
551 (last access: 12 June 2024). Our results can be made available upon request.

552

553 **Author contributions.** JF and FLX conceptualized and designed the research. FLX and JF
554 synthesized and analyzed the data. FLX, SW, YL, and JF produced the figures. FLX and SW
555 contributed to the datasets retrieval. All the authors discussed the results and wrote the paper.

556 **Competing interests.** The authors declare that they have no conflict of interest.

557

558 **Disclaimer.** Publisher's note: Copernicus Publications remains neutral with regard to jurisdictional
559 claims in published maps and institutional affiliations.

560

561 **Acknowledgements.** The authors would like to thank two anonymous reviewers for their useful
562 comments that contributed to improving the manuscript. This work was jointly supported by the
563 National Natural Science Foundation of China (42222501) and the BNU-FGS Global
564 Environmental Change Program (No. 2023-GC-ZYTS-03).

565

References

- 567 Abid, M. A., Kucharski, F., Molteni, F., Kang, I.-S., Tompkins, A. M., and Almazroui, M.: Separating the Indian and
 568 Pacific Ocean Impacts on the Euro-Atlantic Response to ENSO and Its Transition from Early to Late Winter, *J.*
 569 *Climate*, 34, 1531–1548, <https://doi.org/10.1175/JCLI-D-20-0075.1>, 2021.
- 570 Achakulwisut, P., Shen, L., and Mickley, L. J.: What Controls Springtime Fine Dust Variability in the Western United
 571 States? Investigating the 2002–2015 Increase in Fine Dust in the U.S. Southwest, *J. Geophys. Res.-Atmos.*, 122,
 572 <https://doi.org/10.1002/2017JD027208>, 2017.
- 573 Ayarzagüena, B., Ineson, S., Dunstone, N. J., Baldwin, M. P., and Scaife, A. A.: Intraseasonal Effects of El Niño–
 574 Southern Oscillation on North Atlantic Climate, *J. Climate*, 31, 8861–8873, <https://doi.org/10.1175/JCLI-D-18-0097.1>, 2018.
- 576 Cai, W. J., Santoso, A., Collins, M., Dewitte, B., Karamperidou, C., Kug, J.-S., Lengaigne, M., McPhaden, M. J.,
 577 Stuecker, M. F., Taschetto, A. S., Timmermann, A., Wu, L. X., Yeh, S.-W., Wang, G. J., Ng, B., Jia, F., Yang, Y.,
 578 Ying, J., Zheng, X. T., Bayr, T., Brown, J. R., Capotondi, A., Cobb, K. M., Gan, B. L., Geng, T., Ham, Y.-G.,
 579 Jin, F. F., Jo, H.-S., Li, X. C., Lin, X. P., McGregor, S., Park, J.-H., Stein, K., Yang, K., Zhang, L., and Zhong,
 580 W. X.: Changing El Niño–Southern Oscillation in a warming climate, *Nat. Rev.-Earth Environ.*, 2, 628–644,
 581 <https://doi.org/10.1038/s43017-021-00199-z>, 2021.
- 582 Chen, S. F., Wu, R. G., and Chen, W.: Strengthened Connection between Springtime North Atlantic Oscillation and
 583 North Atlantic Tripole SST Pattern since the Late 1980s, *J. Climate*, 35, 2007–2022,
 584 <https://doi.org/10.1175/JCLI-D-19-0628.1>, 2020.
- 585 Chen, S. F., Chen W., Xie, S. P., Yu, B., Wu, R. G., Wang, Z. B., Lan, X. Q., and Graf, H.: Strengthened impact of
 586 boreal winter North Pacific Oscillation on ENSO development in warming climate, *npj Climate and*
 587 *Atmospheric Science*, 7, 69, <https://doi.org/10.1038/s41612-024-00615-3>, 2024.
- 588 Chen, S.Y., Zhao, D., Huang, J. P., He, J. Q., Chen, Y., Chen, J. Y., Bi, H. R., Lou, G. T., Du, S. K., Zhang, Y., and
 589 Yang, F.: Mongolia Contributed More than 42% of the Dust Concentrations in Northern China in March and
 590 April 2023, *Adv. Atmos. Sci.*, 40, 1549–1557, <https://doi.org/10.1007/s00376-023-3062-1>, 2023.
- 591 Csavina, J., Field, J., Félix, O., Corral-Avitia, A. Y., Sáez, A. E., and Betterton, E. A.: Effect of wind speed and
 592 relative humidity on atmospheric dust concentrations in semi-arid climates, *Sci. Total Environ.*, 487, 82–90,
 593 <https://doi.org/10.1016/j.scitotenv.2014.03.138>, 2014.
- 594 Ding, R. Q., Nnamchi, H. C., Yu, J. Y., Li, T., Sun, C., Li, J. P., Tseng, Y., Li, X. C., Xie, F., Feng, J., Ji, K., and Li,
 595 X. M.: North Atlantic oscillation controls multidecadal changes in the North Tropical Atlantic–Pacific
 596 connection, *Nat. Commun.*, 14, 862, <https://doi.org/10.1038/s41467-023-36564-3>, 2023.
- 597 Fan, K., Xie, Z. M., Wang, H. J., Xu, Z. Q., and Liu, J. P.: Frequency of spring dust weather in North China linked
 598 to sea ice variability in the Barents Sea, *Clim. Dyn.*, 51, 4439–4450, <https://doi.org/10.1007/s00382-016-3515-7>, 2018.
- 600 Feldstein, S. B.: The dynamics of NAO teleconnection pattern growth and decay, *Q. J. Roy. Meteor. Soc.*, 129, 901–
 601 924, <https://doi.org/10.1256/qj.02.76>, 2003.
- 602 Feng, J. and Li, J. P.: Influence of El Niño Modoki on spring rainfall over south China, *J. Geophys. Res.-Atmos.*,
 603 116, D13102, <https://doi.org/10.1029/2010JD015160>, 2011.
- 604 Feng, J., Li, J. P., Liao, H., and Zhu, J. L.: Simulated coordinated impacts of the previous autumn North Atlantic
 605 Oscillation (NAO) and winter El Niño on winter aerosol concentrations over eastern China, *Atmos. Chem.*
 606 *Phys.*, 19, 10787–10800, <https://doi.org/10.5194/acp-19-10787-2019>, 2019.
- 607 Feng, J., Zhu, J. L., Li, J. P., and Liao, H.: Aerosol concentrations variability over China: two distinct leading modes,
 608 *Atmos. Chem. Phys.*, 20, 9883–9893, <https://doi.org/10.5194/acp-20-9883-2020>, 2020.

609 Gelaro, R., McCarty, W., Suárez, M. J., Todling, R., Molod, A., Takacs, L., Randles, C. A., Darmenov, A., Bosilovich,
610 M. G., Reichle, R., Wargan, K., Coy, L., Cullather, R., Draper, C., Akella, S., Buchard, V., Conaty, A., Da Silva,
611 A. M., Gu, W., Kim, G.-K., Koster, R., Lucchesi, R., Merkova, D., Nielsen, J. E., Partyka, G., Pawson, S.,
612 Putman, W., Rienecker, M., Schubert, S. D., Sienkiewicz, M., and Zhao, B.: The Modern-Era Retrospective
613 Analysis for Research and Applications, Version 2 (MERRA-2), *J. Climate*, 30, 5419–5454,
614 <https://doi.org/10.1175/JCLI-D-16-0758.1>, 2017.

615 Gong, S. L., Zhang, X. Y., Zhao, T. L., Zhang, X. B., Barrie, L. A., McKendry, I. G., and Zhao, C. S.: A Simulated
616 Climatology of Asian Dust Aerosol and Its Trans-Pacific Transport. Part II: Interannual Variability and Climate
617 Connections, *J. Climate*, 19, 104–122, <https://doi.org/10.1175/JCLI3606.1>, 2006.

618 Guo, Y., Li, J. P., and Li, Y.: A Time-Scale Decomposition Approach to Statistically Downscale Summer Rainfall
619 over North China, *J. Climate*, 25, 572–591, <https://doi.org/10.1175/JCLI-D-11-00014.1>, 2012.

620 Hersbach, H., Bell, B., Berrisford, P., Hirahara, S., Horányi, A., Muñoz-Sabater, J., Nicolas, J., Peubey, C., Radu, R.,
621 Schepers, D., Simmons, A., Soci, C., Abdalla, S., Abellan, X., Balsamo, G., Bechtold, P., Biavati, G., Bidlot, J.,
622 Bonavita, M., De Chiara, G., Dahlgren, P., Dee, D., Diamantakis, M., Dragani, R., Flemming, J., Forbes, R.,
623 Fuentes, M., Geer, A., Haimberger, L., Healy, S., Hogan, R. J., Hólm, E., Janisková, M., Keeley, S., Laloyaux,
624 P., Lopez, P., Lupu, C., Radnoti, G., De Rosnay, P., Rozum, I., Vamborg, F., Villaume, S., and Thépaut, J.: The
625 ERA5 global reanalysis, *Q. J. Roy. Meteor. Soc.*, 146, 1999–2049, <https://doi.org/10.1002/qj.3803>, 2020.

626 Hu, Z. Y., Ma, Y. Y., Jin, Q. J., Idrissa, N. F., Huang, J. P., and Dong, W. J.: Attribution of the March 2021 exceptional
627 dust storm in North China, *B. Am. Meteorol. Soc.*, 104, E749–E755, <https://doi.org/10.1175/BAMS-D-22-0151.1>, 2023.

629 Huang, J., Li, Y., Fu, C., Chen, F., Fu, Q., Dai, A., Shinoda, M., Ma, Z., Guo, W., Li, Z., Zhang, L., Liu, Y., Yu, H.,
630 He, Y., Xie, Y., Guan, X., Ji, M., Lin, L., Wang, S., Yan, H., and Wang, G.: Dryland climate change: Recent
631 progress and challenges, *Rev. Geophys.*, 55, 719–778, <https://doi.org/10.1002/2016RG000550>, 2017.

632 Huang, J. P., Liu, J. J., Chen, B., and Nasiri, S. L.: Detection of anthropogenic dust using CALIPSO lidar
633 measurements, *Atmos. Chem. Phys.*, 15, 11653–11665, <https://doi.org/10.5194/acp-15-11653-2015>, 2015.

634 Huang, Y. H., Liu, X. D., Yin, Z., and An, Z. S.: Global Impact of ENSO on Dust Activities with Emphasis on the
635 Key Region from the Arabian Peninsula to Central Asia, *J. Geophys. Res.-Atmos.*, 126, e2020JD034068,
636 <https://doi.org/10.1029/2020JD034068>, 2021.

637 Hurrell, J. W.: Decadal Trends in the North Atlantic Oscillation: Regional Temperatures and Precipitation, *Science*,
638 269, 676–679, <https://doi.org/10.1126/science.269.5224.676>, 1995.

639 Ji, L. Q. and Fan, K.: Climate prediction of dust weather frequency over northern China based on sea-ice cover and
640 vegetation variability, *Clim. Dyn.*, 53, 687–705, <https://doi.org/10.1007/s00382-018-04608-w>, 2019.

641 Jia, X. J., Derome, J., and Lin, H.: Comparison of the Life Cycles of the NAO Using Different Definitions, *J. Climate*,
642 20, 5992–6011, <https://doi.org/10.1175/2007JCLI1408.1>, 2007.

643 Jiang, W. P., Huang, G., Huang, P., Wu, R. G., Hu, K. M., and Chen, W.: Northwest Pacific Anticyclonic Anomalies
644 during Post-El Niño Summers Determined by the Pace of El Niño Decay, *J. Climate*, 32, 3487–3503,
645 <https://doi.org/10.1175/JCLI-D-18-0793.1>, 2019.

646 Jiménez-Esteve, B. and Domeisen, D. I. V.: The Tropospheric Pathway of the ENSO–North Atlantic Teleconnection,
647 *J. Climate*, 31, 4563–4584, <https://doi.org/10.1175/JCLI-D-17-0716.1>, 2018.

648 Jones, P. D., Jonsson, T., and Wheeler, D.: Extension to the North Atlantic Oscillation using early instrumental
649 pressure observations from Gibraltar and South-West Iceland. *Int. J. Climatol.*, 17, 1433–1450,
650 [https://doi.org/10.1002/\(SICI\)1097-0088\(19971115\)17:13<1433::AID-JOC203>3.0.CO;2-P](https://doi.org/10.1002/(SICI)1097-0088(19971115)17:13<1433::AID-JOC203>3.0.CO;2-P), 1997.

651 Kang, L. T., Huang, J. P., Chen, S. Y., and Wang, X.: Long-term trends of dust events over Tibetan Plateau during
652 1961–2010, *Atmos. Environ.*, 125, 188–198, <https://doi.org/10.1016/j.atmosenv.2015.10.085>, 2016.

653 Ke, M. L., Wang, Z. Q., Pan, W. J., Luo, H. L., Yang, S., and Guo, R. Y.: Extremely Strong Western Pacific
654 Subtropical High in May 2021 Following a La Niña Event: Role of the Persistent Convective Forcing over the
655 Indian Ocean, *Asia-pac. J. Atmos. Sci.*, 59, 47–58, <https://doi.org/10.1007/s13143-022-00300-6>, 2023.

656 Kim, H. and Choi, M.: Impact of soil moisture on dust outbreaks in East Asia: Using satellite and assimilation data,
657 *Geophys. Res. Lett.*, 42, 2789–2796, <https://doi.org/10.1002/2015GL063325>, 2015.

658 Kim, S. and Kug, J.: What Controls ENSO Teleconnection to East Asia? Role of Western North Pacific Precipitation
659 in ENSO Teleconnection to East Asia, *J. Geophys. Res.-Atmos.*, 123, <https://doi.org/10.1029/2018JD028935>,
660 2018.

661 Kok, J. F., Storelvmo, T., Karydis, V. A., Adebisi, A. A., Mahowald, N. M., Evan, A. T., He, C. L., and Leung, D.
662 M.: Mineral dust aerosol impacts on global climate and climate change, *Nat. Rev.-Earth Environ.*, 4, 71–86,
663 <https://doi.org/10.1038/s43017-022-00379-5>, 2023.

664 Li, J. P., and Wang, J. X. L.: A new North Atlantic Oscillation index and its variability, *Adv. Atmos. Sci.*, 20, 661–
665 676, <https://doi.org/10.1007/BF02915394>, 2003.

666 Li, J. P., Zheng, F., Sun, C., Feng, J., and Wang, J.: Pathways of Influence of the Northern Hemisphere Mid-high
667 Latitudes on East Asian Climate: A Review, *Adv. Atmos. Sci.*, 36, 902–921, <https://doi.org/10.1007/s00376-019-8236-5>, 2019.

669 Li, J., Carlson, B. E., Yung, Y. L., Lv, D., Hansen, J., Penner, J. E., Liao, H., Ramaswamy, V., Kahn, R. A., Zhang,
670 P., Dubovik, O., Ding, A. J., Lacis, A. A., Zhang, L., and Dong, Y. M.: Scattering and absorbing aerosols in the
671 climate system, *Nat. Rev.-Earth Environ.*, 3, 363–379, <https://doi.org/10.1038/s43017-022-00296-7>, 2022.

672 Li, Y., Xu, F. L., Feng, J., Du, M. Y., Song, W. J., Li, C., and Zhao, W. J.: Influence of the previous North Atlantic
673 Oscillation (NAO) on the spring dust aerosols over North China, *Atmos. Chem. Phys.*, 23, 6021–6042,
674 <https://doi.org/10.5194/acp-23-6021-2023>, 2023.

675 Liu, X. D., Yin, Z., Zhang, X. Y., and Yang, X. C.: Analyses of the spring dust storm frequency of northern China in
676 relation to antecedent and concurrent wind, precipitation, vegetation, and soil moisture conditions, *J. Geophys.*
677 *Res.-Atmos.*, 109, 2004JD004615, <https://doi.org/10.1029/2004JD004615>, 2004.

678 López-Parages, J., Rodríguez-Fonseca, B., and Terray, L.: A mechanism for the multidecadal modulation of ENSO
679 teleconnection with Europe, *Clim. Dyn.*, 45, 867–880, <https://doi.org/10.1007/s00382-014-2319-x>, 2015.

680 Lou, S. J., Russell, L. M., Yang, Y., Xu, L., Lamjiri, M. A., DeFlorio, M. J., Miller, A. J., Ghan, S. J., Liu, Y., and
681 Singh, B.: Impacts of the East Asian Monsoon on springtime dust concentrations over China, *J. Geophys. Res.-*
682 *Atmos.*, 121, 8137–8152, <https://doi.org/10.1002/2016JD024758>, 2016.

683 Lou, S. J., Russell, L. M., Yang, Y., Liu, Y., Singh, B., and Ghan, S. J.: Impacts of interactive dust and its direct
684 radiative forcing on interannual variations of temperature and precipitation in winter over East Asia, *J. Geophys.*
685 *Res.-Atmos.*, 122, 8761–8780, <https://doi.org/10.1002/2017JD027267>, 2017.

686 McPhaden, M. J. and Zhang, X. B.: Asymmetry in zonal phase propagation of ENSO sea surface temperature
687 anomalies, *Geophys. Res. Lett.*, 36, 2009GL038774, <https://doi.org/10.1029/2009GL038774>, 2009.

688 Pan, L. L.: Observed positive feedback between the NAO and the North Atlantic SSTA tripole, *Geophys. Res. Lett.*,
689 32, 2005GL022427, <https://doi.org/10.1029/2005GL022427>, 2005.

690 Prospero, J. M., Nees, R. T., and Uematsu, M.: Deposition rate of particulate and dissolved aluminum derived from
691 saharan dust in precipitation at Miami, Florida, *J. Geophys. Res.-Atmos.*, 92, 14723–14731,
692 <https://doi.org/10.1029/JD092iD12p14723>, 1987.

693 Rayner, N. A., Parker, D. E., Horton, E. B., Folland, C. K., Alexander, L. V., Rowell, D. P., Kent, E. C., and Kaplan,
694 A.: Global analyses of sea surface temperature, sea ice, and night marine air temperature since the late
695 nineteenth century, *J. Geophys. Res.-Atmos.*, 108, 2002JD002670, <https://doi.org/10.1029/2002JD002670>,
696 2003.

697 Shao, T. B., Liu, Y. Z., Tan, Z. Y., Li, D., Luo, M., and Luo, R.: Characteristics and a mechanism of dust weather in
698 Northern China, *Clim. Dyn.*, 61, 1591–1606, <https://doi.org/10.1007/s00382-022-06644-z>, 2023.

699 Song, L. Y., Chen, S. F., Chen, W., Guo, J. P., Cheng, C. L., and Wang, Y.: Distinct evolutions of haze pollution from
700 winter to following spring over the North China Plain: Role of the North Atlantic sea surface temperature
701 anomalies. *Atmos. Chem. Phys.*, 22, 1669–1688, <https://doi.org/10.5194/acp-22-1669-2022>, 2022.

702 Su, J. Z., Zhang, R. H., Li, T., Rong, X. Y., Kug, J., and Hong, C.: Causes of the El Niño and La Niña Amplitude
703 Asymmetry in the Equatorial Eastern Pacific, *J. Climate*, 23, 605–617, <https://doi.org/10.1175/2009JCLI2894.1>,
704 2010.

705 Sung, M., Lim, G., and Kug, J.: Phase asymmetric downstream development of the North Atlantic Oscillation and
706 its impact on the East Asian winter monsoon, *J. Geophys. Res.-Atmos.*, 115, 2009JD013153,
707 <https://doi.org/10.1029/2009JD013153>, 2010.

708 Takaya, K. and Nakamura, H.: A Formulation of a Phase-Independent Wave-Activity Flux for Stationary and
709 Migratory Quasigeostrophic Eddies on a Zonally Varying Basic Flow, *J. Atmospheric Sci.*, 58, 608–627,
710 [https://doi.org/10.1175/1520-0469\(2001\)058<0608:AFOAPI>2.0.CO;2](https://doi.org/10.1175/1520-0469(2001)058<0608:AFOAPI>2.0.CO;2), 2001.

711 Trenberth, K. E.: The Definition of El Niño, *B. Am. Meteorol. Soc.*, 78, 2771–2777, [https://doi.org/10.1175/1520-0477\(1997\)078<2771:TDOENO>2.0.CO;2](https://doi.org/10.1175/1520-0477(1997)078<2771:TDOENO>2.0.CO;2), 1997.

713 Wallace, J. M. and Gutzler, D. S.: Teleconnections in the Geopotential Height Field during the Northern Hemisphere
714 Winter, *Mon. Weather Rev.*, 109, 784–812, [https://doi.org/10.1175/1520-0493\(1981\)109<0784:TITGHF>2.0.CO;2](https://doi.org/10.1175/1520-0493(1981)109<0784:TITGHF>2.0.CO;2), 1981.

716 Wang, B., Wu, R. G., and Fu, X. H.: Pacific–East Asian Teleconnection: How Does ENSO Affect East Asian
717 Climate?, *J. Climate*, 13, 1517–1536, [https://doi.org/10.1175/1520-0442\(2000\)013<1517:PEATHD>2.0.CO;2](https://doi.org/10.1175/1520-0442(2000)013<1517:PEATHD>2.0.CO;2),
718 2000.

719 Wang, C., Ren, B. H., Li, G., Zheng, J. Q., Jiang, L. W., and Xu, D.: An Interdecadal Change in the Influence of the
720 NAO on Atlantic-Induced Arctic Daily Warming around the Mid-1980s, *Adv. Atmos. Sci.*, 40, 1285–1297,
721 <https://doi.org/10.1007/s00376-022-2218-8>, 2023.

722 Wang, T. H., Tang, J. Y., Sun, M. X., Liu, X. W., Huang, Y. X., Huang, J. P., Han, Y., Cheng, Y. F., Huang, Z. W., and
723 Li, J. M.: Identifying a transport mechanism of dust aerosols over South Asia to the Tibetan Plateau: A case
724 study, *Sci. Total Environ.*, 758, 11, <https://doi.org/10.1016/j.scitotenv.2020.143714>, 2021.

725 Wang, Z. Q., Yang, S., Lau, N.-C., and Duan, A. M.: Teleconnection between Summer NAO and East China Rainfall
726 Variations: A Bridge Effect of the Tibetan Plateau, *J. Climate*, 31, 6433–6444, <https://doi.org/10.1175/JCLI-D-17-0413.1>, 2018.

728 Woollings, T., Franzke, C., Hodson, D. L. R., Dong, B., Barnes, E. A., Raible, C. C., and Pinto, J. G.: Contrasting
729 interannual and multidecadal NAO variability, *Clim. Dyn.*, 45, 539–556, <https://doi.org/10.1007/s00382-014-2237-y>, 2015.

731 Wu, B., Zhou, T. J., and Li, T.: Atmospheric Dynamic and Thermodynamic Processes Driving the Western North
732 Pacific Anomalous Anticyclone during El Niño. Part I: Maintenance Mechanisms, *J. Climate*, 30, 9621–9635,
733 <https://doi.org/10.1175/JCLI-D-16-0489.1>, 2017.

734 Wu, J., Kurosaki, Y., Shinoda, M., and Kai, K.: Regional Characteristics of Recent Dust Occurrence and Its
735 Controlling Factors in East Asia, *Sola*, 12, 187–191, <https://doi.org/10.2151/sola.2016-038>, 2016.

736 Wu, R. G. and Chen, S. F.: What Leads to Persisting Surface Air Temperature Anomalies from Winter to Following
737 Spring over Mid- to High-Latitude Eurasia? *J. Climate*, 33, 5861–5883, <https://doi.org/10.1175/JCLI-D-19-0819.1>, 2020.

739 Wu, Z. W., Wang, B., Li, J. P., and Jin, F. F.: An empirical seasonal prediction model of the east Asian summer
740 monsoon using ENSO and NAO, *J. Geophys. Res.-Atmos.*, 114, 2009JD011733,
741 <https://doi.org/10.1029/2009JD011733>, 2009.

742 Wu, Z. W., Li, J. P., Jiang, Z. H., He, J. H., and Zhu, X. Y.: Possible effects of the North Atlantic Oscillation on the
743 strengthening relationship between the East Asian Summer monsoon and ENSO, *Int. J. Climatol.*, 32, 794–800,
744 <https://doi.org/10.1002/joc.2309>, 2012.

745 Xi, X. and Sokolik, I. N.: Dust interannual variability and trend in Central Asia from 2000 to 2014 and their climatic
746 linkages, *J. Geophys. Res.-Atmos.*, 120, <https://doi.org/10.1002/2015JD024092>, 2015.

747 Yang, Y., Zeng, L. Y., Wang, H. L., Wang, P. Y., and Liao, H.: Dust pollution in China affected by different spatial
748 and temporal types of El Niño, *Atmos. Chem. Phys.*, 22, 14489–14502, [https://doi.org/10.5194/acp-22-14489-](https://doi.org/10.5194/acp-22-14489-2022)
749 [2022](https://doi.org/10.5194/acp-22-14489-2022), 2022a.

750 Yang, Y., Li, M. Y., Wang, H. L., Li, H. M., Wang, P. Y., Li, K., Gao, M., and Liao, H.: ENSO modulation of
751 summertime tropospheric ozone over China, *Environ. Res. Lett.*, 17, 034020, [https://doi.org/10.1088/1748-](https://doi.org/10.1088/1748-9326/ac54cd)
752 [9326/ac54cd](https://doi.org/10.1088/1748-9326/ac54cd), 2022b.

753 Yao, W. R., Gui, K., Wang, Y. Q., Che, H. Z., and Zhang, X. Y.: Identifying the dominant local factors of 2000–2019
754 changes in dust loading over East Asia, *Sci. Total Environ.*, 777, 146064,
755 <https://doi.org/10.1016/j.scitotenv.2021.146064>, 2021.

756 Yu, Y., Notaro, M., Liu, Z. Y., Wang, F. Y., Alkolibi, F., Fadda, E., and Bakhrjy, F.: Climatic controls on the
757 interannual to decadal variability in Saudi Arabian dust activity: Toward the development of a seasonal dust
758 prediction model, *J. Geophys. Res.-Atmos.*, 120, 1739–1758, <https://doi.org/10.1002/2014JD022611>, 2015.

759 Zhang, P., Wu, Z. W., and Jin, R.: How can the winter North Atlantic Oscillation influence the early summer
760 precipitation in Northeast Asia: effect of the Arctic sea ice, *Clim. Dyn.*, 56, 1989–2005,
761 <https://doi.org/10.1007/s00382-020-05570-2>, 2021a.

762 Zhang, R. H., Li, T. R., Wen, M., and Liu, L. K.: Role of intraseasonal oscillation in asymmetric impacts of El Niño
763 and La Niña on the rainfall over southern China in boreal winter, *Clim. Dyn.*, 45, 559–567,
764 <https://doi.org/10.1007/s00382-014-2207-4>, 2015.

765 Zhang, R. H., Tian, W. S., He, X., Qie, K., Liu, D., and Tian, H. Y.: Enhanced influence of ENSO on winter
766 precipitation over southern China in recent decades, *J. Climate*, 1–36, [https://doi.org/10.1175/JCLI-D-21-](https://doi.org/10.1175/JCLI-D-21-0182.1)
767 [0182.1](https://doi.org/10.1175/JCLI-D-21-0182.1), 2021b.

768 Zhang, W. J., Li, J. P., and Jin, F. F.: Spatial and temporal features of ENSO meridional scales, *Geophys. Res. Lett.*,
769 36, 2009GL038672, <https://doi.org/10.1029/2009GL038672>, 2009.

770 Zhang, W. J., Li, H. Y., Stuecker, M. F., Jin, F. F., and Turner, A. G.: A New Understanding of El Niño’s Impact over
771 East Asia: Dominance of the ENSO Combination Mode, *J. Climate*, 29, 4347–4359,
772 <https://doi.org/10.1175/JCLI-D-15-0104.1>, 2016.

773 Zhang, X. Y., Gong, S. L., Zhao, T. L., Arimoto, R., Wang, Y. Q., and Zhou, Z. J.: Sources of Asian dust and role of
774 climate change versus desertification in Asian dust emission, *Geophys. Res. Lett.*, 30, 2003GL018206,
775 <https://doi.org/10.1029/2003GL018206>, 2003.

776 Zhao, C. F., Yang, Y. K., Fan, H., Huang, J. P., Fu, Y. F., Zhang, X. Y., Kang, S. C., Cong, Z. Y., Letu, H., and Menenti,
777 M.: Aerosol characteristics and impacts on weather and climate over the Tibetan Plateau, *Natl. Sci. Rev.*, 7,
778 492–495, <https://doi.org/10.1093/nsr/nwz184>, 2020.

779 Zhao, S., Li, J. P., and Sun, C.: Decadal variability in the occurrence of wintertime haze in central eastern China tied
780 to the Pacific Decadal Oscillation, *Sci. Rep.*, 6, 27424, <https://doi.org/10.1038/srep27424>, 2016.

781 Zhao, Y., Huang, A. N., Zhu, X. S., Zhou, Y., and Huang, Y.: The impact of the winter North Atlantic Oscillation on
782 the frequency of spring dust storms over Tarim Basin in northwest China in the past half-century, *Environ. Res.*
783 *Letts.*, 8, 024026, <https://doi.org/10.1088/1748-9326/8/2/024026>, 2013.

784 Zheng, F., Li, J. P., Li, Y. J., Zhao, S., and Deng, D. F.: Influence of the Summer NAO on the Spring-NAO-Based
785 Predictability of the East Asian Summer Monsoon, *J. Appl. Meteorol. Clim.*, 55, 1459–1476,
786 <https://doi.org/10.1175/JAMC-D-15-0199.1>, 2016a.

787 Zheng, Y., Zhao, T. L., Che, H. Z., Liu, Y., Han, Y. X., Liu, C., Xiong, J., Liu, J. H., and Zhou, Y. K.: A 20-year
788 simulated climatology of global dust aerosol deposition, *Sci. Total Environ.*, 557–558, 861–868,
789 <https://doi.org/10.1016/j.scitotenv.2016.03.086>, 2016b.

790 Zhou, F., Shi, J., Liu, M. H., and Ren, H. C.: Linkage between the NAO and Siberian high events on the intraseasonal
791 timescale, *Atmos. Res.*, 281, 106478, <https://doi.org/10.1016/j.atmosres.2022.106478>, 2023.

792 Zhu, C. W., Wang, B., and Qian, W. H.: Why do dust storms decrease in northern China concurrently with the recent
793 global warming? *Geophys. Res. Letts.*, 35, 2008GL034886, <https://doi.org/10.1029/2008GL034886>, 2008.

794 Zuo, J. Q., Ren, H. L., Li, W. J., and Wang, L.: Interdecadal Variations in the Relationship between the Winter North
795 Atlantic Oscillation and Temperature in South-Central China, *J. Climate*, 29, 7477–7493,
796 <https://doi.org/10.1175/JCLI-D-15-0873.1>, 2016.